COMPASS physics program: present and future

COMPASS,...
CEA Saclay, DSM/IRFU/SPhN

May 7, 2014

Contents

Part I

Spin Physics at COMPASS

Part II

GPD program at COMPASS

The COMPASS-II program [1] was accepted by the SPS scientific committee at CERN in 2010. It is mainly focused on the studies of Generalised Parton Distributions (GPDs) and the Transverse Momentum Dependent parton distributions (TMD PDFs or TMDs). These two types of functions aim for the most complete description of the partonic structure of the nucleon. They can be considered as different projections of generalised parton correlation functions [2] which have a direct connection to the Wigner distributions - the quantum mechanical analogues of classical phase space distributions - of the hadron-parton system. While the standard PDFs give only information on the longitudinal nucleon momentum fraction carried by the parton, GPDs and TMDs provide a 3-dimensional information of the nucleon, either in a mixed (transverse) position - (longitudinal) momentum representation for the former or in a pure momentum representation for the latter. Moreover, they contain important information on the orbital motion of partons inside the nucleon.

TMDs are studied at COMPASS in semi-inclusive deep inelastic scattering (SIDIS) using the 160 GeV high-energy muon beam scattered off polarized proton (NH_3) and deuteron (^6LiD) targets. They will be further investigated for the first time ever in the polarized Drell-Yan process in 2014-15 using the 190 GeV pion beam and a transversely polarized proton target.

The GPD program, initiated by the SPhN team, aims to put experimental constraints on GPDs using hard exclusive reactions such as deeply virtual Compton scattering (DVCS) and hard exclusive meson production (HEMP) with the muon beam. The addition of a recoil proton detector to the existing COMPASS spectrometer is mandatory at these high energies to select only exclusive events.

In the following sections, the goal of the accepted DVCS program using positive and negative polarized muon beams and an unpolarized proton (LH_2) target is described. The different steps to achieve such a measurement with a recoil proton detection are outlined: first test measurements in 2008-09, a pilot run of four weeks in 2012 with the recoil detector CAMERA, and the preparation of the two years data taking in 2016-17. Next, results on the hard exclusive ρ production obtained during the SIDIS measurements with a transversely polarized target, but without recoil detection are also presented. Finally, first ideas for possible DVCS and HEMP measurements using a recoil detector surrounding a transversely polarized target for measurements at COMPASS beyond 2018 are given.

1 The DVCS program with recoil detection and LH_2 target

1.1 Motivations

With the 160 GeV muon beam available at CERN, the DVCS measurements cover a kinematic domain defined by the momentum fraction, x_{Bj}, ranging from 0.01 to 0.15 and by the photon virtuality, Q^2, between 1 and 10 GeV^2. A comparison with the domains covered by several other experiments is shown in Fig. 1. COMPASS will thus explore the uncharted x_{Bj} domain between the HERA collider experiments H1 [3] and ZEUS [4] and the fixed-target experiments as HERMES [5] and JLab [6, 7]. We note that JLab is presently the only other active laboratory.

The DVCS process interferes with the Bethe-Heitler (BH) process due to identical final

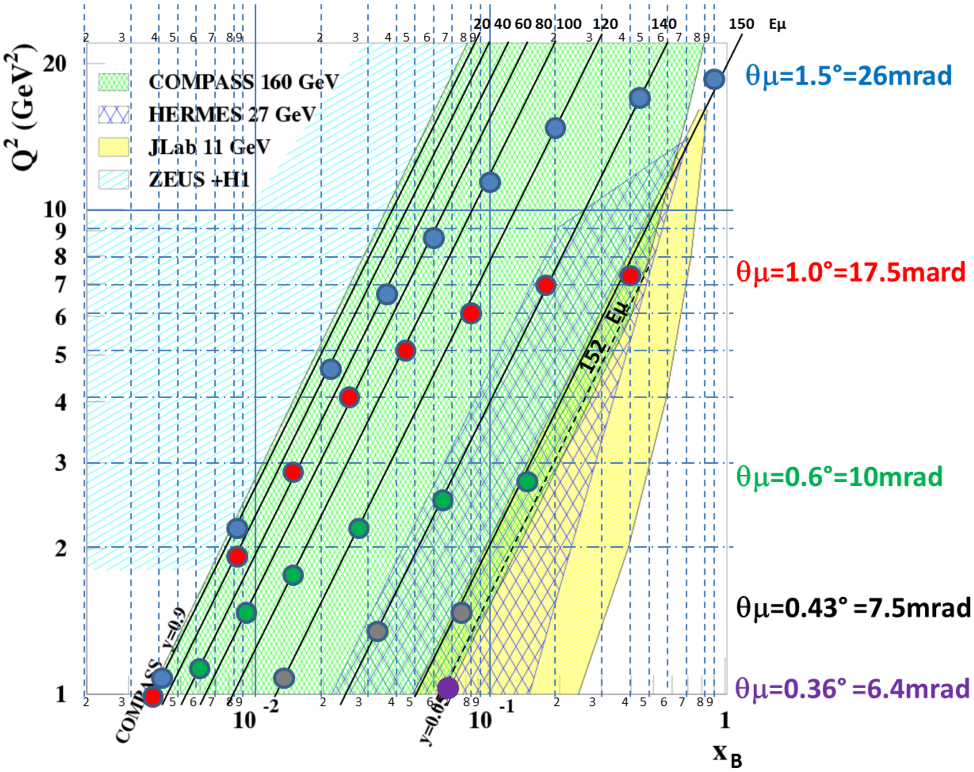

Figure 1: The (Q^2, x_{Bj}) kinematic domain (in green) covered by COMPASS for $y = (E_\mu - E_{\mu'})/E_\mu$ ranging from 0.9 to 0.05. The colored circles indicate each a different outgoing muon angle.

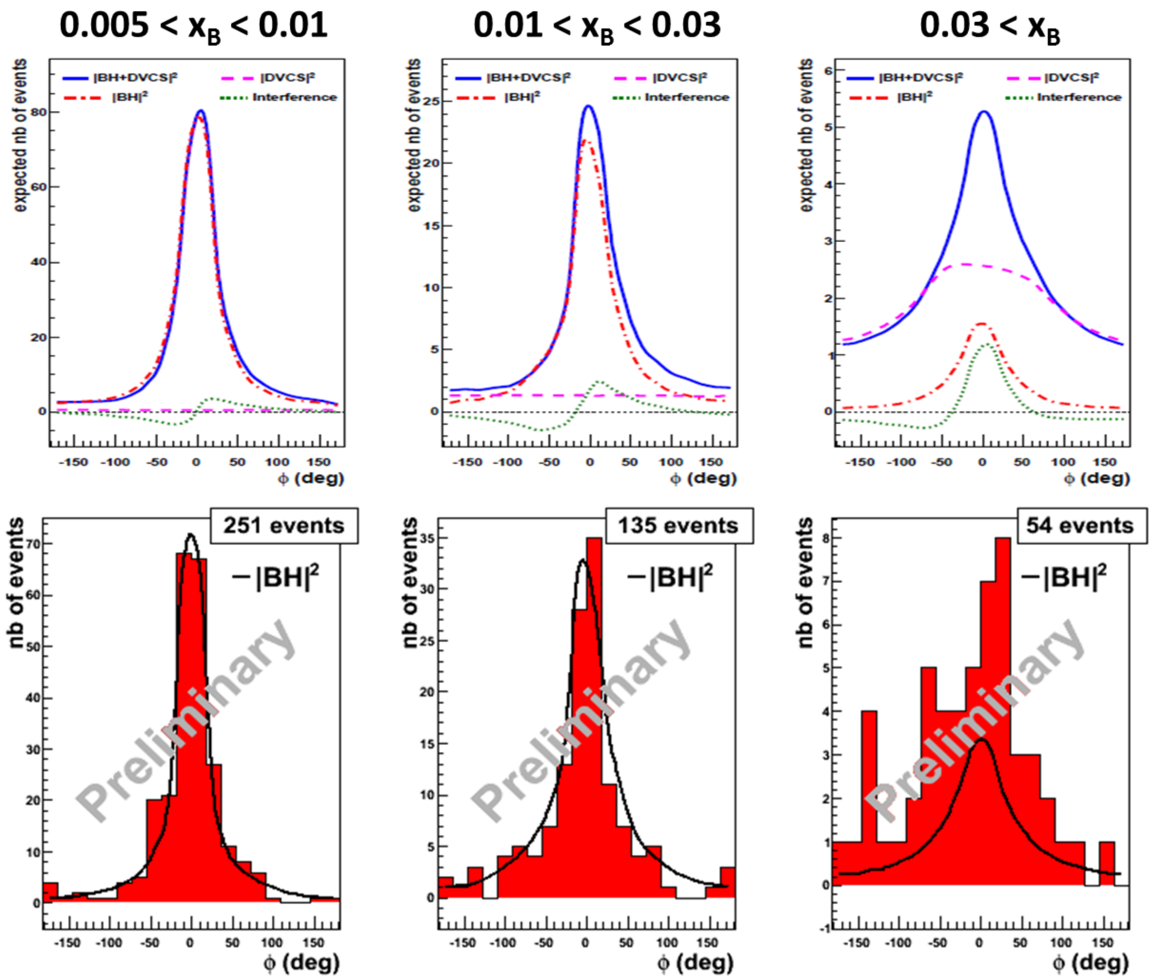

Figure 2: **Top:** Monte Carlo simulation of the exclusive muoproduction of a single real photon at COMPASS-II with only the 2 existing calorimeters ECAL1 and ECAL2 showing the ϕ angle distributions of reconstructed events for three bins in x_B for $Q^2 > 1$ GeV^2. **Bottom:** ϕ angle distributions measured in the DVCS 2009 test run. The solid lines represent the expected BH yield.

states. The cross-section for hard exclusive muoproduction of a single photon off an unpolarized proton is written as:

$$\frac{\mathrm{d}^4\sigma(\mu p \to \mu p \gamma)}{\mathrm{d}x_B \mathrm{d}Q^2 \mathrm{d}|t| \mathrm{d}\phi} = \mathrm{d}\sigma^{BH} + \mathrm{d}\sigma_0^{DVCS} + P_\mu \, \mathrm{d}\Delta\sigma^{DVCS} + e_\mu \mathrm{Re}\, I + e_\mu P_\mu \, \mathrm{Im}\, I, \tag{1}$$

where P_μ and e_μ are the polarization and the charge of the muon beam, and I denotes the DVCS-BH interference term. Here, t is the four-momentum transfer squared between the initial and final nucleon states and ϕ is the angle between the scattering plane and the photon production plane. Figure 2 (top) shows a Monte Carlo simulation with the different contributions for $Q^2 > 1$ GeV^2 based on the acceptance of the standard COMPASS spectrometer, *i.e.*, using only the existing electromagnetic calorimeters ECAL1 and ECAL2. An important feature of the calculation is the large dominance of the BH contribution for $x_{Bj} < 0.01$. Since this process is known, it provides an excellent reference for monitoring the detector acceptance and the luminosity measurement. The size of the interference term increases with rising x_{Bj} and offers via its characteristic ϕ modulation additional possibilities to access real and imaginary part of the complex DVCS amplitude. The DVCS process itself is dominant for $x_{Bj} > 0.03$. The distribution for DVCS is not flat in ϕ due to the limited acceptance at large photon angles if we use only ECAL1 and ECAL2. This justify the implementation of the new electromagnetic calorimeter ECAL0 to enlarge the photon acceptance.

From the previous equation one can build the sum $\mathcal{S}$ and the difference $\mathcal{D}$ of the cross-sections for a simultaneous change of charge and polarization of the incoming lepton beam ($+$ to $-$ and $\leftarrow$ to $\rightarrow$):

$$\mathcal{D} \equiv \mathrm{d}\sigma^{\overset{+}{\leftarrow}} - \mathrm{d}\sigma^{\overset{-}{\rightarrow}} = 2[\mathrm{d}\Delta\sigma^{DVCS} + \mathrm{Re}\, I] \xrightarrow{L.T.} c_0^I + c_1^I \cos\phi \tag{2}$$

$$\mathcal{S} \equiv \mathrm{d}\sigma^{\overset{+}{\leftarrow}} + \mathrm{d}\sigma^{\overset{-}{\rightarrow}} = 2[\mathrm{d}\sigma^{BH} + \mathrm{d}\sigma_0^{DVCS} + \mathrm{Im}\, I] \xrightarrow{L.T.} 2\mathrm{d}\sigma^{BH} + c_0^{DVCS} + s_1^I \sin\phi \tag{3}$$

The muon beam used at COMPASS has such a property: the negative muons have a polarization opposite to that of the positive muons. Eqs. 2 and 3 indicate also the harmonic terms in the azimuthal angular decomposition at twist-two level (or leading twist, noted L.T.). With a proton target in the COMPASS kinematics, the coefficients c_i^j or s_i^j are related to the dominant Compton form factor (CFF) $\mathcal{H}$, which is a convolution of the GPD H with a hard kernel describing the photon-quark interaction [8].

Upon integration over the azimuthal angle ϕ, the interference contribution to $\mathcal{S}$ vanishes. After subtraction of the BH contribution one obtains the pure DVCS cross-section. The latter depends on the squared momentum transfer t from the initial to the final nucleon. If the behavior $\mathrm{d}\sigma_0^{DVCS}/\mathrm{d}t \propto \exp(-B(x_{Bj})|t|)$ is confirmed with the data, and using the relation $< r_\perp^2(x_{Bj}) > \approx 2B(x_{Bj})$ valid at small x_{Bj}, the transverse distance, $r_\perp$, between the struck quark and the center of mass of the spectator system can be extracted. The measurement of the transverse nucleon size obtained is thus independent of any GPD parametrization. A projection of the uncertainties expected after 280 days of data taking is displayed in Fig. 3. A comparison with the results obtained at HERA [3, 4] at similar $\langle Q^2 \rangle$ but lower x_{Bj} is also shown.

The ϕ dependence of the difference $\mathcal{D}$ (Eq. 2), the sum $\mathcal{S}$ (Eq. 3), and the asymmetry $\mathcal{A} = \mathcal{D}/\mathcal{S}$ allow for the extraction of quantities related to the CFF $\mathcal{H}$ and thus constrain the GPD H. The statistics expected in two years of data taking will enable the measurement of six bins in x_{Bj} ranging from 0.005 to 0.3, six bins in t ranging from 0.06 to 0.7 GeV^2 and

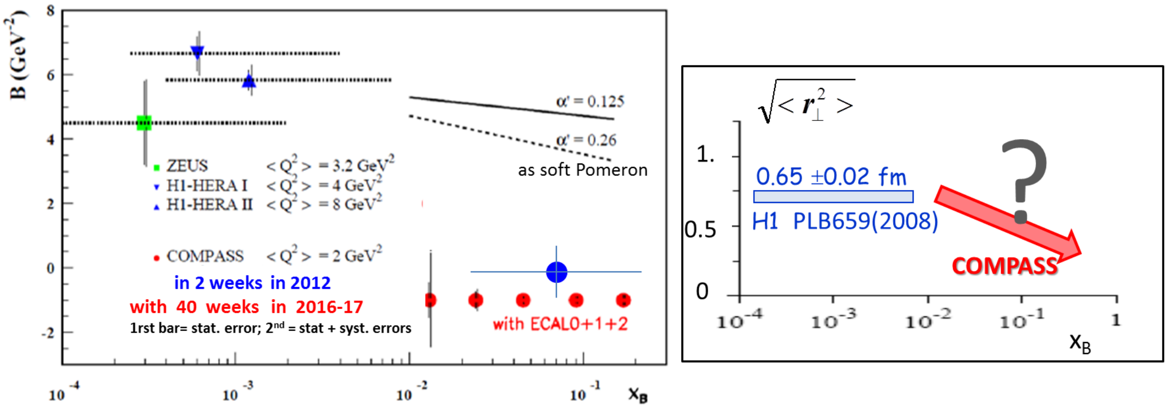

Figure 3: **Left:** Projections for measuring the x_{Bj} dependence of the t-slope parameter $B(x_{Bj})$ of the DVCS cross section, calculated for $1 < Q^2 < 8$ GeV^2. The left vertical bar on each red data point indicates the projected statistical error, while the right one includes also the systematic uncertainty. The parametrization $B(x_{Bj}) = B_0 + 2\,\alpha' \log(\frac{x_0}{x_{Bj}})$ is shown using two values of α', 0.125 GeV^{-2} and 0.26 GeV^{-2} corresponding respectively to the half and to the total of the value of a Pomeron exchange in soft scattering processes. **Right:** Transverse proton radius as a function of x_{Bj}.

four bins in Q^2 from 1 to 16 GeV^2. Figure 4 presents the $\cos\phi$ modulation of the asymmetry, integrated over Q^2 as a function of t in the six bins of x_{Bj}. This modulation is related to the real part of the CFF $\mathcal{H}$. Note that the real and imaginary parts of the CFF are related by a dispersion relation requiring a subtraction D-term. The D-term, related to the confinement of partons in the nucleon, is not well constrained by the present data. The real part of the CFF $\mathcal{H}$ was found positive at HERA and negative at HERMES. The kinematic domain of COMPASS, in particular the region $0.005 < x_{Bj} < 0.03$ (see the top panels of Fig. 4) is expected to allow the determination of the x_{Bj} position of the node of this function, which is important for any global fitting procedure.

1.2 2008-2009 DVCS test measurements

In 2008 and 2009, test measurements were performed using the COMPASS spectrometer in a configuration optimized for the hadron spectroscopy program. A 40 cm long liquid hydrogen target surrounded by a 1 m long Recoil Proton Detector (RPD) was used. This setup provided the configuration of the future experiment but at a smaller scale (length of the target and the recoil detector reduced by a factor 6 and 4, respectively). In addition, the large angle electromagnetic calorimeter ECAL0 was not yet available.

The first short run in 2008 has proved the capability of the apparatus to detect and reconstruct exclusive single photon events. Approximately 10 times more events were collected in 2009. The exclusive single photon production reaction $\mu p \to \mu' \gamma p'$ is selected by applying cuts on the missing energy:

$$E_{miss} = (M^2_{miss} - M^2_p)/2M_p \tag{4}$$

and the differences:

$$\Delta\phi = \phi_{miss} - \phi_{RPD} \quad \text{and} \quad \Delta p_T = |p_T^{miss}| - |p_T^{RPD}|, \tag{5}$$

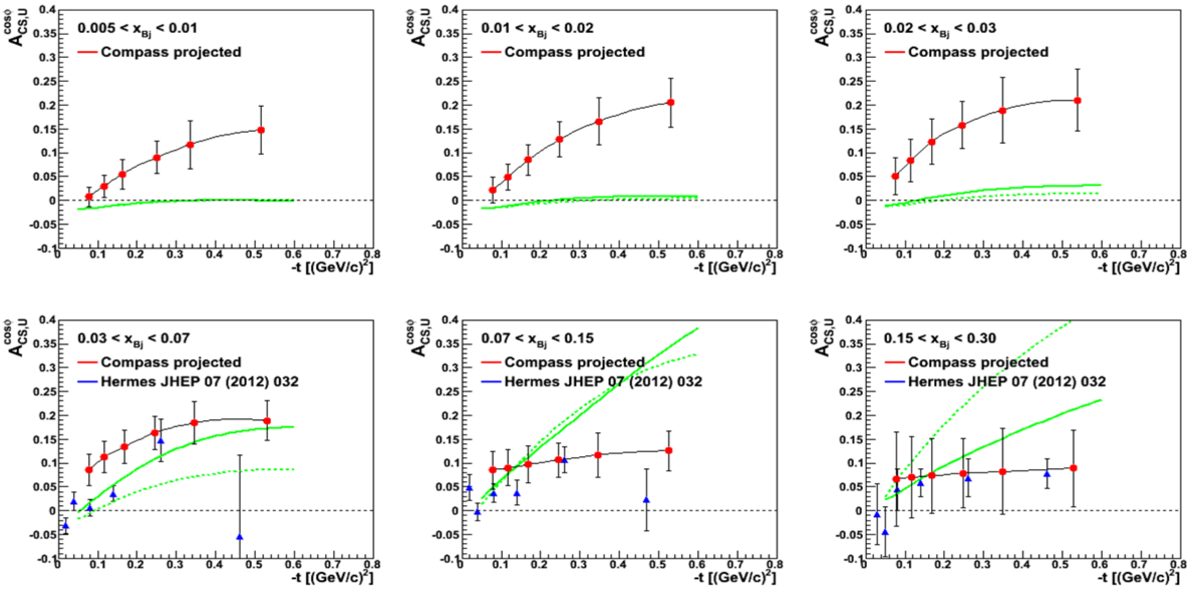

Figure 4: Projected statistical accuracy for the amplitude of the cosϕ modulation of the beam charge and spin asymmetry. Projections (red points) are calculated using the reggeized variant of the VGG model [9]. The blue triangles show the HERMES results [5]. The green curves show the latest predictions [10] based on the first fit on world data with (solid line), or without (dotted line) JLab Hall A data.

where the missing particle defined by $\vec{P_{miss}} = \vec{P_\mu} - \vec{P_{\mu'}} - \vec{P_\gamma}$ should be a proton of mass M_p, and where p_T denotes the momentum in the transverse plane with respect to the incident muon direction and ϕ the azimuthal angle around this direction.

This analysis gives access to the ϕ distributions in three bins in x_{Bj} presented in the lower part of the Fig. 2. The solid lines represent the expected BH contribution, while the histogram shows the measured single photon yields. The latter include both BH and pure DVCS events, as well as misidentified π^0 events.

The efficiency to detect muons in coincidence with a proton and a photon was evaluated to be 35% in the bin of the smallest x_{Bj}, where the BH contribution is dominant. After taking into account DAQ dead time, veto dead times, and SPS and spectrometer live times, the efficiency is further reduced by about a factor 0.8^4. Its final value is compatible with the global efficiency of 10% used in the predictions. Furthermore, a luminosity determination with a systematic accuracy of 5% was also obtained and cross checked with the known values of the F_2 structure function which parametrizes the DIS cross section.

The main background to DVCS is due to the detection of only one of the two photons from π^0 decay (the other photon is undetected due to acceptance or absorption). Estimation of this background was done using a full chain MC with two generators: HEPGEN [11] for exclusive π^0 production and LEPTO for semi-inclusive π^0 production. The total background contamination at large x_{Bj} was estimated to be smaller than one third of the total number of events after BH subtraction.

Seven internal COMPASS notes on exclusivity, ϕ distributions, luminosity, π^0 contamination have been written between 2009 and 2013. This work is part of the PhD thesis of Marie Boer.

1.3 2012 DVCS pilot run

A first measurement of the exclusive single photon production ($\mu p \to \mu' \gamma p'$) was performed at the end of 2012 using the 160 GeV high-energy muon beam and the full scale setup, as it will be used in 2016-17. The full scale setup (see Fig. 5) comprises a 2.5 m long liquid Hydrogen (LH_2) target, a new 4 m long recoil detector named CAMERA, and a new electromagnetic calorimeter ECAL0, which extends the angular acceptance for photon detection. The apparatus used in 2012 is shown in Fig. 6. The CAMERA detector was built swiftly in 18 months after the SPSC approval. After commissioning of the new detectors, four weeks of DVCS data were collected.

1.3.1 Liquid hydrogen target

The 2.5m long liquid Hydrogen (LH_2) target was designed and constructed by the CERN Cryolab. The Carbon fiber vacuum chamber surrounding the target was provided by the Yamagata group. The target is installed on a rail system fixed to the CAMERA structure. The hydrogen pressure stability is about 30 mbar around the operational pressure of 1130 mbar. The pressure stability results in a variation of the liquid hydrogen density below 0.1%.

1.3.2 Electromagnetic calorimeters

A new electromagnetic calorimeter, ECAL0, was designed in order to extend the available photon acceptance towards large angles. ECAL0 is under construction at JINR, Dubna. A part of it, consisting of 56 modules (about 25% of total), was placed 1.5 m downstream of the LH_2 target for the data taking in 2012. The ECAL0 modules are equipped with multichannel avalanche photon detectors (MAPD), temperature stabilization, and a LED-based monitoring system. Prior to the data taking, the modules were tested with cosmic muons. An inter-calibration of the modules was performed using the wide muon beam halo. A calibration of ECAL0 was performed using the π^0 produced by the 190 GeV/c π^- beam impinging on the LH_2 target. The calibration coefficients were determined by reconstructing the π^0 mass peak from its two-photon decay, and comparing it to its nominal value, as illustrated in Fig. 7 (top). The width of the peak is fully given by energy and spatial resolution of the calorimeter and it is about 10 MeV.

In order to match the angular acceptance of ECAL1 to that of ECAL2, the size of the central hole of ECAL1 was reduced, both horizontally and vertically. To carry out this size reduction, 208 new, radiation-hard, Shashlik modules were installed in ECAL1. After π^0 calibration, π^0 widths of 10 and 5 MeV are observed in the invariant mass $\gamma\gamma$ spectrum of ECAL1 and ECAL2, respectively (see Fig. 7 (middle) and (bottom)).

During the analysis of the data collected, many ECAL1 modules were found to be particularly noisy. Figure 8 (left) shows the factor R, which is the ratio between the number of events correlated with the trigger time and the number of random events in each module of ECAL1. R varies from 4 for good cells to 0.1 for bad cells in the central part of ECAL1. As a comparison, typical values of R of 7 for ECAL0 and 9 for ECAL2 are obtained, even for photon energies as low as 1 GeV. An elaborated method based on a Fourier transform analysis of the pulse shape was developed in order to extract the precise amplitude and time of the signal. After Fourier analysis, the values of R increase to 45 and 13 for the good and bad cells, respectively. The impact of the Fourier analysis is illustrated in Fig. 8. This method is now being used to analyze all ECAL1 data collected in 2012.

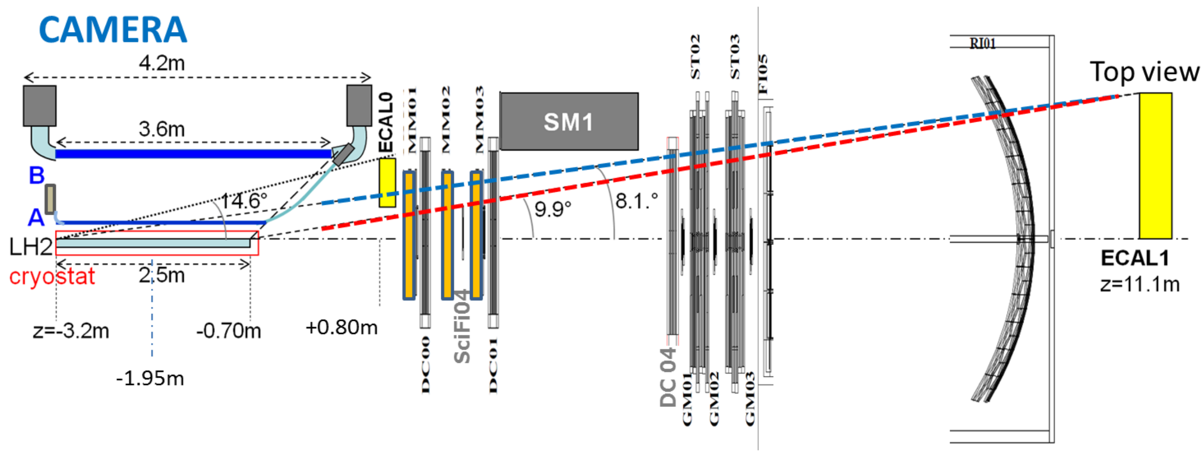

Figure 5: A schema of the COMPASS setup around the target.

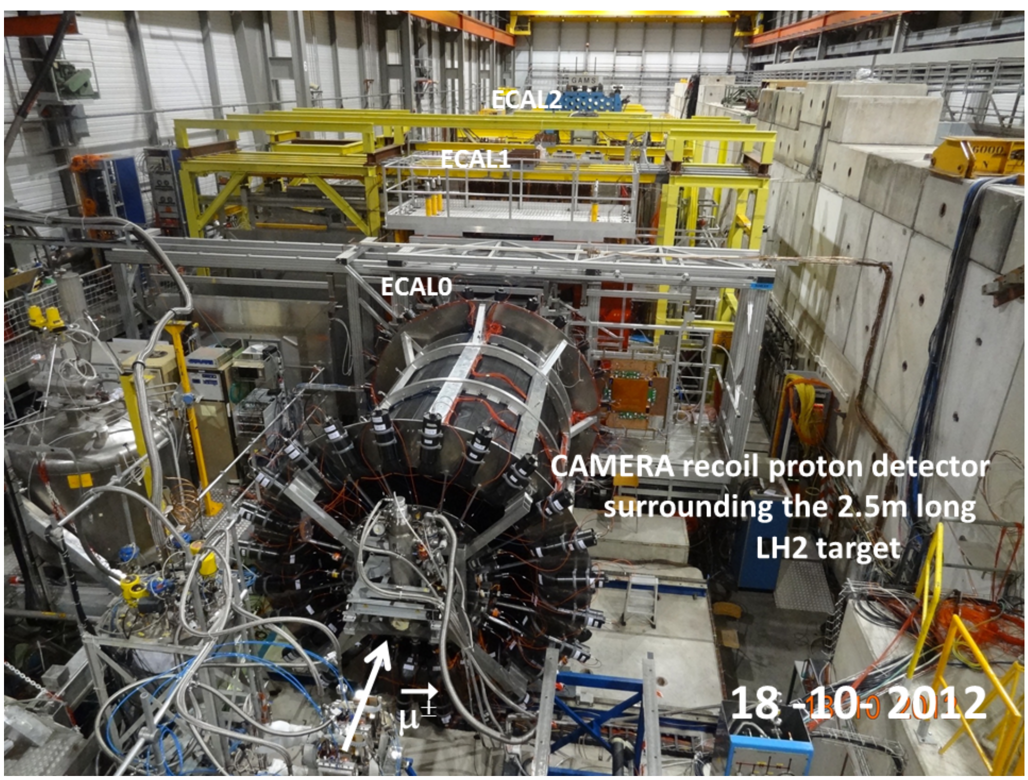

Figure 6: Picture taken on 2012-10-18 presenting the recoil proton detector CAMERA installed around the 2.5m LH_2 target just before ECAL0 and the complete COMPASS spectrometer.

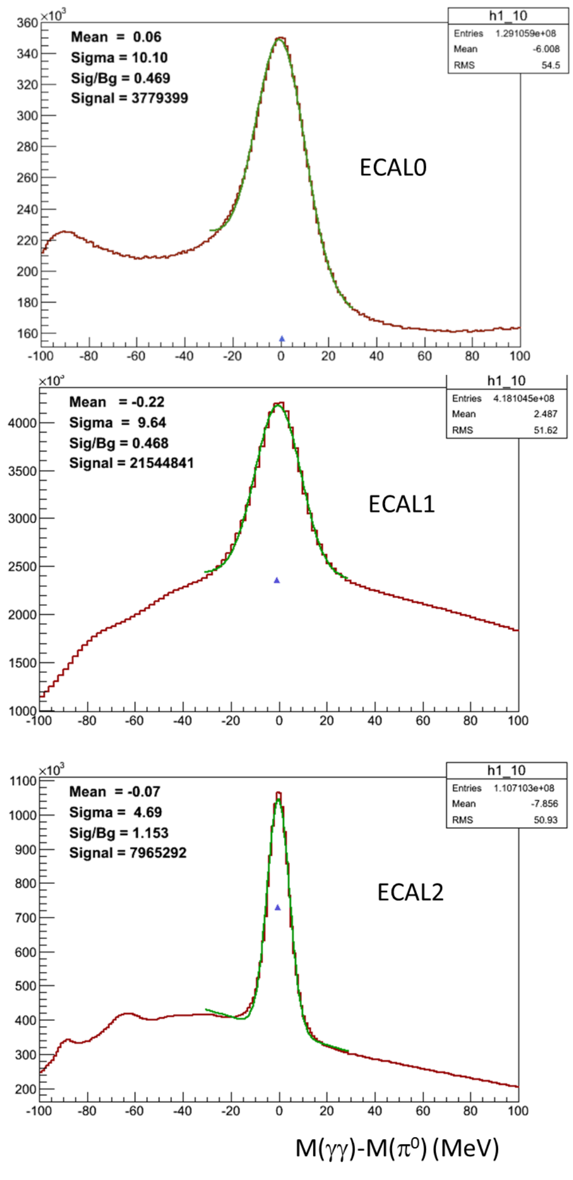

Figure 7: π^0 peak in the invariant mass $\gamma\gamma$ spectrum (MeV) obtained after calibration with the pion beam for ECAL0 (top), ECAL1 (middle), and ECAL2 (bottom).

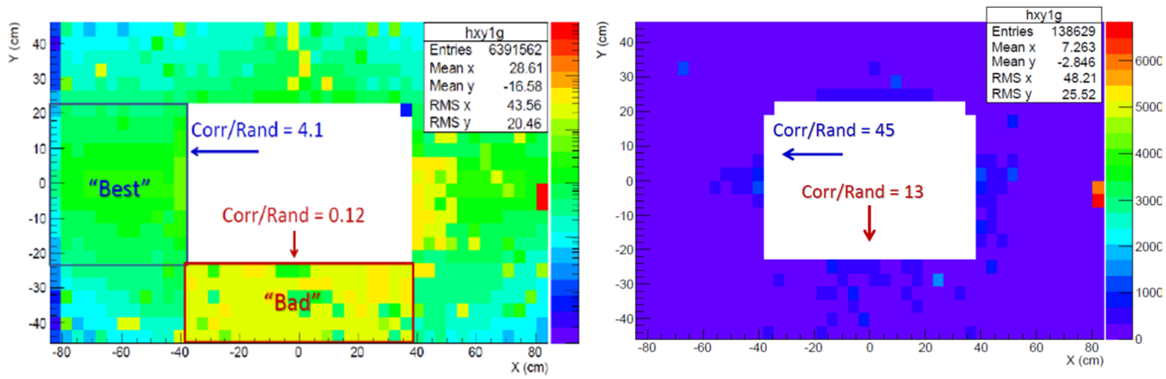

Figure 8: Factor R of number of correlated events over the number of random events in each module of the central part of ECAL1, before and after the Fourier analysis of the pulse shape.

1.3.3 Pixel Micromegas detectors

Figure 19 shows the detectors between the target and the first dipole magnet SM1. In 2012, they consisted in two large area trackers (drift chambers DC00 and DC01), 12 small area trackers (Micromegas stations MM01, MM02, MM03) and one very small area tracker (scintillating fiber station SCiFi04). In order to complete the very small area tracker, two new Micromegas detectors, equipped with pixels in the center, were installed. With only two active pixel MM detectors, the tracking suffers from a lack of redundancy needed to remove the combinatorial background. The impact of the additional angular coverage corresponding to outgoing muon angles smaller than 10 mrad can be observed in the DVCS kinematic domain as illustrated in Fig. 1.

1.3.4 Recoil proton detector

The new large recoil proton detector, CAMERA, is based on a Time of Flight (ToF) measurement between two barrels of 24 scintillators read at both ends. Figure 9 shows the insertion of the inner barrel inside the outer one. The outer barrel, noted B, with a diameter of 2.2 m is made of 3.6 m long and 5 cm thick scintillators. The inner barrel A has a diameter of 50 cm. It is made of 2.75 m long and 4 mm thick scintillators. The design of CAMERA and of the target with its environment allows detection of proton momentum as low as 270 MeV/c. The thin and long scintillating slabs of the inner barrel are equipped with long light guides on the downstream side in order to minimize the material budget in the forward acceptance region, as illustrated in Fig. 5. This makes the project really challenging in order to achieve the expected timing resolution of 310 ps. Such a timing resolution provides a proton momentum resolution varying from 4% to 10% and equivalently a t resolution varying from 8% to 20% when the proton momentum increases from 300 to 700 MeV/c. Such a resolution is mandatory to build six bins in t for an accurate determination of the t-dependence of the DVCS cross section.

Accounting the weakness of the inner ring A and developing successful methods for the precise ToF determination are really more complex tasks than expected for different reasons which will be given below. Presently, final results are not yet available.

Table 1: Properties of the scintillators slabs of MUREX and CAMERA detectors.

	MUREX		CAMERA	
	A	B	A	B
material	BC408	BC408	BC408	BC408
thickness (cm)	0.4	5	0.4	5
length (cm)	284	400	275	360
PMT	XP20H0	XP4512	ET9813B	ET9823B
light guide	twisted	fish tail	bend and twisted	optimized bend shape 3D machining
attenuation length (cm)	210	320	70-120	265-305
time resolution (ps)	270	160	350	160
ToF resolution (ps)	310		not yet finalized	

New readout with the GANDALF system. The event readout is done with the GANDALF system, developed in Freiburg University. GANDALF collects the signals from the Photo Multiplier Tubes (PMTs) with a sampling at 1 GHz and provides their amplitudes corrected for time and amplitude dependence, using a constant fraction algorithm implemented in its FPGA. The difference and the sum of the time information collected at both ends of a scintillator represent, after final calibration, the position and the time, respectively, of the particle track crossing the scintillator. The proton momentum is determined from the evaluated velocity $\beta = DoF/(c \cdot ToF)$ where DoF and ToF are the distance and the time of flight of the proton between the inner and outer rings.

GANDALF is used for the first time for a ToF measurement. In order to achieve the best possible time resolution, certain corrections have to be applied to the raw data. In particular, the effects of small deviations of the signal baseline as well as of the precise signal shape have been addressed very recently. Although this work is still in progress, the preliminary results are very encouraging.

Bad attenuation length and poor timing resolution of the inner ring. Time resolution and attenuation length of each element were measured prior to the data taking, using cosmic rays. In Table 1, the properties of A and B elements used in CAMERA are compared to the properties of the prototypes of same size, MUREX, built in 2006. The attenuation lengths λ are close to 2.8 m for the scintillators B, while they are spread around 0.9 m for the scintillators A (see Figs. 10 and 11). The values for scintillators A compare unfavorably with the attenuation lengths of about 2 m, measured on the 4 mm thick MUREX prototypes used 6 years earlier. For the data taking in 2012, the best (with $\lambda > 0.9$ m) and worst (with $\lambda < 0.9$ m) scintillators A have been interleaved. The resulting negative impact (shown in the Table) is a timing resolution of 350 ps for the CAMERA inner ring significantly larger than the 270 ps measured for the 4 mm thick MUREX prototypes. This leads to a ToF resolution definitively larger than the expected 310 ps.

Preference for small amplitudes due to PMT anode limitation. The commissioning of CAMERA was done using recoiling protons produced by a pion beam crossing the LH_2 target. Few hours were sufficient to collect enough protons in CAMERA. The final High Voltage (gain) adjustment of the setting of the two PMTs (upstream and downstream) of each scintillator was achieved with the goal of matching the full dynamical range in proton

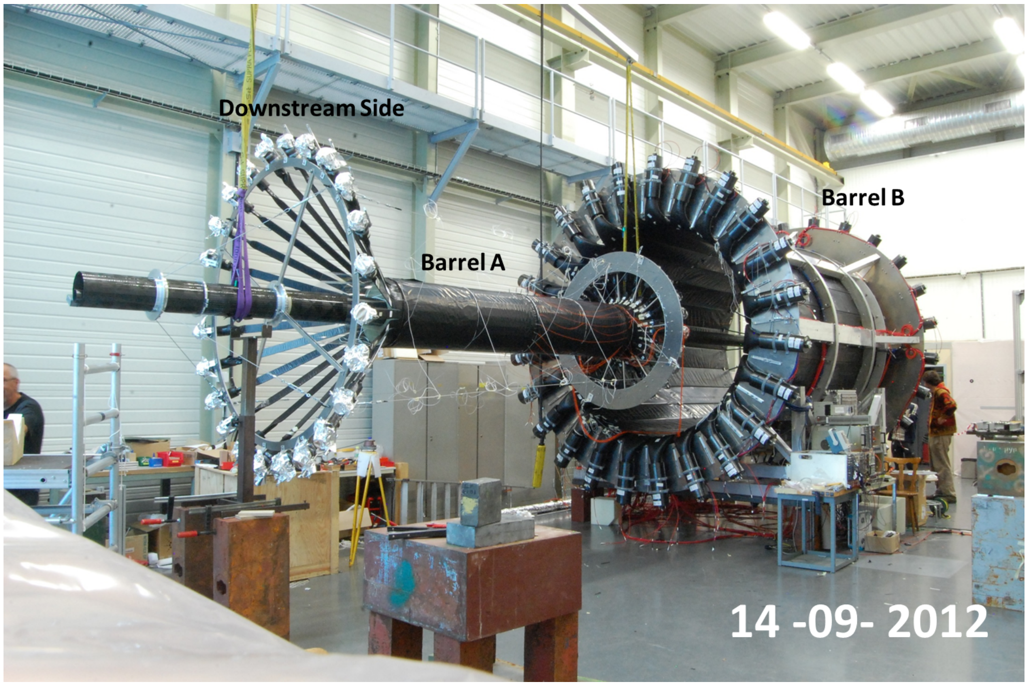

Figure 9: Picture taken on September 14, 2014, showing the insertion of the inner barrel A inside the outer barrel B of CAMERA. The long light guides on the downstream side of the inner barrel are visible on the left side of the picture.

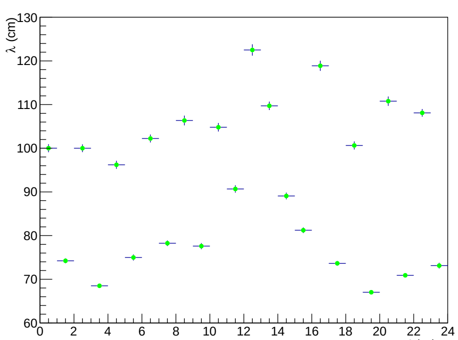

Figure 10: Distribution of attenuation lengths for the 24 scintillators A.

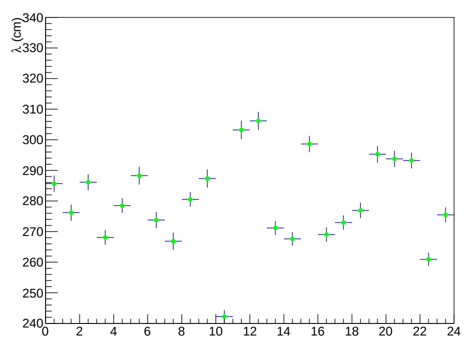

Figure 11: Distribution of attenuation lengths for the 24 scintillators B.

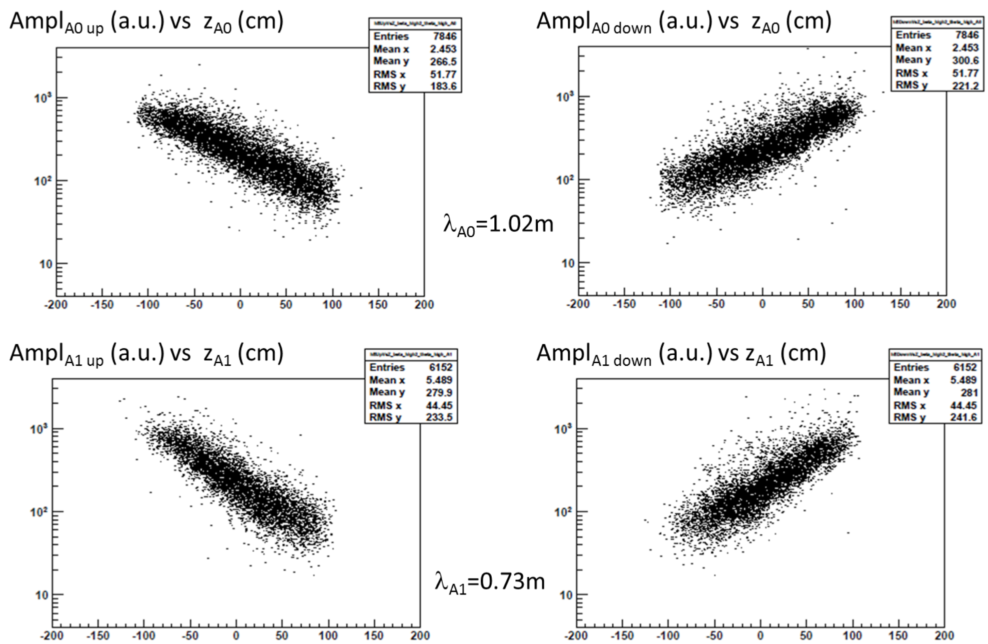

Figure 12: Distribution of the amplitudes collected by the PMTs placed upstream (left) and downstream (right) for A0 (upper part) and for A1 (bottom part) as a function of the position along the scintillator.

momentum. Due to large instantaneous PMT anode currents arising from an important 50 Hz intensity modulation in the 2012 beam spill structure, the HV setting was chosen to minimize the output pulse height. For future running, the Warsaw group is designing an amplifier system on the PMT voltage divider, which will allow to lower the anode current keeping the output pulse height constant (to preserve the dynamical range and maximise the amplitude signal). Figure 12 shows an example of distributions of PMT amplitudes from two of the inner scintillators, a good A0 and a bad A1, versus the position of the hit along the slab. No loss in efficiency for the smallest amplitudes is directly visible. However a precise timing resolution is more difficult to achieve for the smallest amplitudes.

Difficulty to set up a precise timing calibration. The tuning of the time calibration constants can be performed using reactions in which the detection of the forward outgoing particles in the spectrometer determines accurately the recoil proton kinematics. This is the case for either a two-body reaction such as $\pi p \to \pi p$ or a three-body reaction such as $\mu p \to \mu p \rho^0$. Figure 13 shows the proton energy loss in the B barrel as a function of the velocity β of the proton for the two reactions. However, due to the poor resolution for the longitudinal vertex position in the case of two-body reactions at very small angles, and to a large combinatorial background, the elastic pion-proton reaction could not be used in 2012 as it was not able to provide a position accuracy close to 1 cm. Therefore, the $\mu p \to \mu p \rho^0$ reaction has been chosen for the CAMERA calibration. A kinematic fitting procedure has also been developed for this three-body reaction, which greatly improves the accuracy in the determination of the recoiling proton kinematics. The timing calibration can also be performed using extra reference detectors that select relativistic particles (like electrons) crossing both scintillators of CAMERA. The time and position accuracy of the

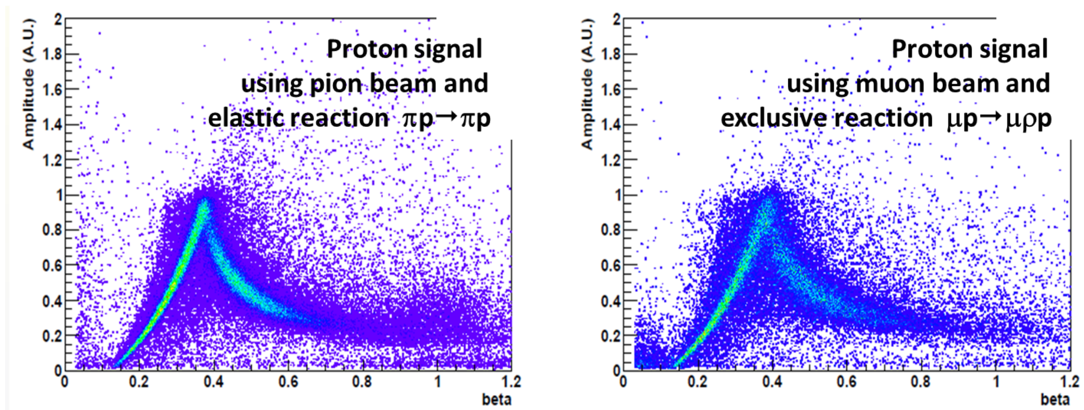

Figure 13: Proton energy loss in the B barrel as a function of the proton velocity β for the reactions $\pi p \to \pi p$ (left) and $\mu p \to \mu \rho^0 p$ (right).

references should be of the order of 100 ps and 1 cm, respectively. This technique was used for the MUREX prototype, and an application to the CAMERA detector is under study (see Section 1.4).

Present status on proton momentum resolution. The momentum resolution $\sigma(dP/P)$ was significantly improved after applying recently the sophisticated time corrections previously discussed in the GANDALF readout section. The corrected values of $\sigma(dP/P)$ vary from 6% at 300 MeV/c to about 13% at 700 MeV/c (Fig. 14 top), instead of the expected 4% at 300 MeV/c and 10% at 700 MeV/c. A small shift of the momentum of about 2% is still present after all corrections for energy losses in the target (Fig. 14 bottom) have been applied. The proton momentum resolution presented in this report is the result of a very recent work, which provides a major step in the understanding of the precise timing determination. However, it has to be cross checked and maybe still improved.

Impact of CAMERA and efficiency The impact of CAMERA on the exclusive reaction $\mu p \to \mu \rho^0 p$ is illustrated in Fig. 15. Without the use of CAMERA the exclusive reaction can be identified by detecting the incident and outgoing muons and the ρ^0 meson using a cut on the missing energy (as Eq. 4). The contribution of non-exclusive events appears on the right of the missing energy peak and increases when the transfer t or the transverse momentum (with respect to the virtual photon direction) p_T of the vector meson ρ^0 increases. Detection of protons in CAMERA allows two additional cuts corresponding to differences between azimuthal angles and between transverse momenta (as Eq. 5). These cuts significantly reduce the non-exclusive background. The resulting efficiency of CAMERA, including the inner ring efficiency, seems reasonably good (about 70%) at low transverse momentum (smaller than 0.8 GeV/c). However this result is not yet reproduced by the sophisticated time analysis and has to be cross checked.

1.3.5 Muon flux determination and stability of the detectors

The DVCS experiment relies on the comparison between measurements made with positive and negative muon beams. An accurate measurement of the corresponding fluxes is therefore necessary. The task, part of the work of the post-doc in Saclay, Eric Fuchey, is somewhat

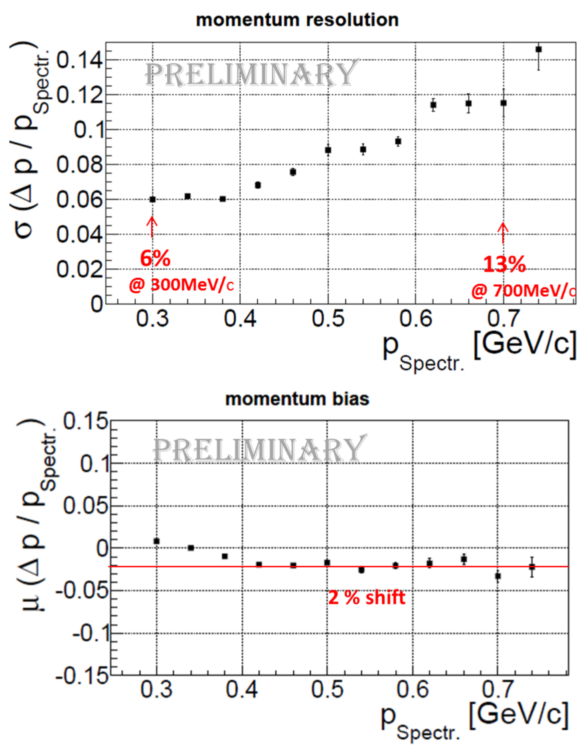

Figure 14: **Top**: Momentum resolution $\sigma(dP/P)$ as a function of the proton momentum. **Bottom**: Shift of the evaluated momentum as a function of the proton momentum.

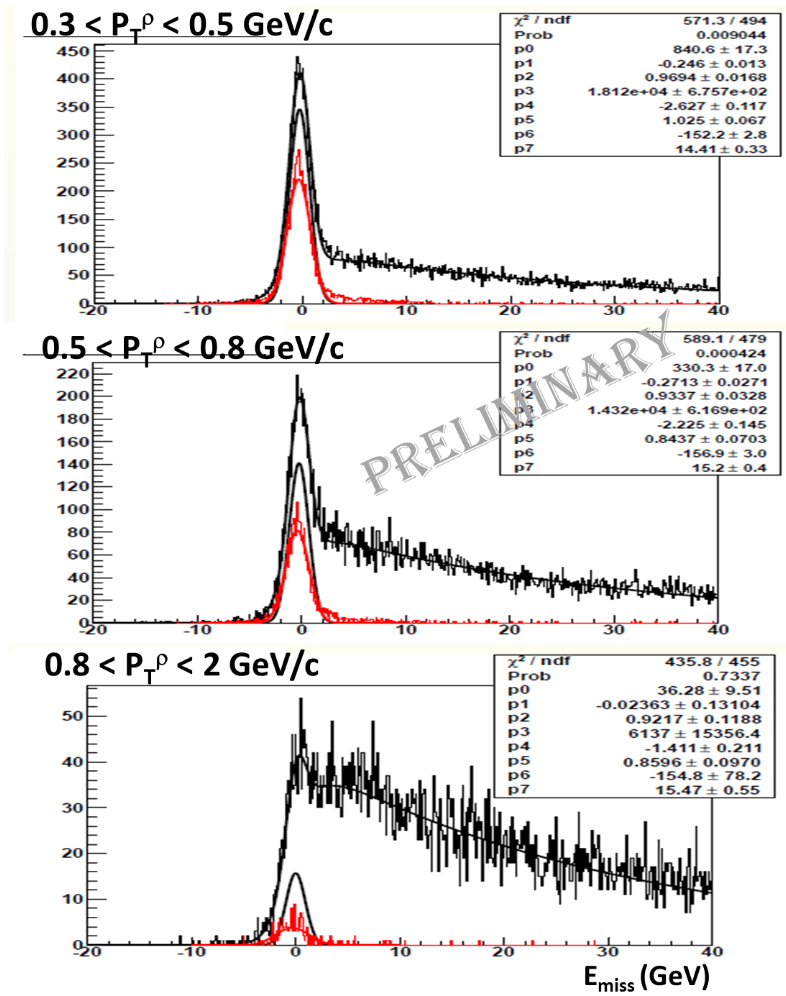

Figure 15: Distribution of $E_{miss}^{\mu p \to \mu \rho^0 X} = (M_{miss}^2 - m_p^2)/2m_p = E_{\gamma *} - E_{\rho^0} + t/2m_p$ presented for three ranges in transverse momentum. The data in black represent exclusive events without using CAMERA, after subtraction of the non-exclusive background. The data in red represent the exclusive events as identified using CAMERA.

complicated, since the positive muon flux is 2.6 times higher than the negative one. The flux determination is performed using beam tracks and a random trigger. The fluxes for both beam polarities are 4.1 $10^8\mu^+$/spill and 1.6 $10^8\mu^-$/spill. Such a high muon flux was never reached for the COMPASS experiment before; it is in perfect agreement with the expected values used in the predictions.

Stability of the semi-inclusive π^0 production yield using μ^+ and μ^- beams is presented in Fig. 16 for a sample of runs taken in one week. The dead times are 0.72 and 0.89 for the μ^+ and μ^- data, respectively. The resulting mean values of the π^0 yield per run for the complete sample of runs along the 4 weeks of data taking are 118.7±1.9 and 119.9±1.9 for the μ^+ and μ^- beams, respectively. This agreement with an accuracy of 2% gives already a first idea of the quality of the monitoring of the experiment.

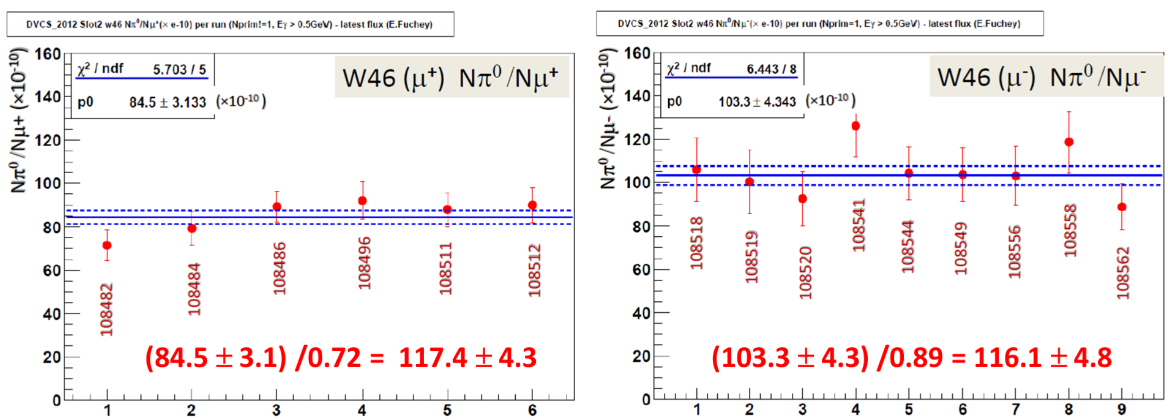

Figure 16: Stability of the semi-inclusive $\pi 0$ production yield per run (indicated with the numbers 108xxx) over one week of data taking with μ^+ and μ^- beams.

1.4 Data taking in 2016-17

Due to the low quality of its scintillators, we do not know yet if the resolution and the efficiency of ring A fulfill our expectations. A final answer can only be given a couple of weeks after full 2012 data set will be produced and analyzed. A decision will then be taken.

An additional Time of Flight (ToF) measurement, can be performed between a high-flux scintillating fiber station placed along the beam axis and the external B ring. Such solution, already partially prepared by the Bonn group during the DVCS2012 data taking, is being studied. Note that the Ring A is still necessary to provide the position resolution.

The ToF resolution at large momentum, i.e. for protons going out of the external ring, should be considerably improved by a layer of Multigap Resistive Plate Chambers (RPC) surrounding the external ring. A prototype, consisting of two rings of 10 cm placed at two longitudinal positions around the external ring, is being considered. It could be made from 1 cm Multigap RPC strips with an appropriate readout. The prototype should be tested during the next data taking and it will provide an excellent online constant calibration system. An European funding has been requested in the framework of the Hadron Physics Horizon 2020 call.

2 Exclusive meson production

Vector meson production provides a complementary tool for accessing the GPDs. Studies of exclusive production of ρ^0 mesons from a transversely polarized target were initiated several years ago. In the absence of a dedicated recoil detector, exclusivity of the reaction $\mu p \to \mu p \rho^0$ is achieved by only a cut on the missing energy (as in Eq. 4), considering the momenta of the incident and scattered muons and the two pions from the ρ^0 decay. The remaining background (about 20%) under the peak is evaluated using a Monte Carlo.

The reaction $\mu p \to \mu p \rho^0$ gives access to the poorly known GPD E and to the chiral odd (or transversity) GPDs H_T and $\bar{E}_T$, which cannot be reached in DVCS. Indeed, for the quark transversity GPDs the emitted and reabsorbed partons have opposite helicities. Since the interactions of light quarks with gluons or photons conserve helicity, the initial parton helicity flip can only be compensated by higher-twist meson wave functions. The GPDs E, H_T and $\bar{E}_T$ are related to the famous Sivers, transversity and Boer-Mulders TMDs.

A transverse polarization of the target allows measurements of the five transverse target single-spin asymmetries A_{UT}, and of the three transverse target double-spin asymmetries A_{LT}. Here, the subscripts U, L, and T mean unpolarized, longitudinally polarized, and transversely polarized respectively, the first subscript referring to the beam, and the second to the target. The angles involved are the azimuthal angle between the lepton scattering plane and the production plane, ϕ, and the azimuthal angle of the transverse target spin vector relative to the lepton scattering plane, ϕ_S. The values of all eight asymmetries depend on x_{Bj}, Q^2 and P_T^2, integrated over the kinematic variables, are shown in Fig. 17.

The asymmetry $A_{UT}^{sin(\phi-\phi_S)}$ (already published, Ref. [12]) is of special interest as it measures the interference term between the GPDs H and E. It is proportional to a weighted sum of convolutions of the GPD $E^{q,g}$ with the distribution amplitude of the produced meson and a hard scattering kernel. The weights depend on the contributions of quarks of various flavors and gluons to the production of a given vector meson. The model of Goloskokov and Kroll [14] explains the small value of the asymmetry as due to an approximate cancellation of two sizable contributions of opposite signs for the GPDs E^u and E^d for the valence u and d quarks, respectively. In contrast, the model predicts larger asymmetries for exclusive production of ω and ρ^+ mesons. Both processes are under study.

The other asymmetries (published in Ref. [13]) are all found compatible with zero, except the asymmetry $A_{UT}^{sin(\phi_S)}$ which deviated from zero by about two standard deviations. This asymmetry is a sum of two interference terms $H \cdot H_T$ and $\bar{E}_T \cdot E$. The asymmetry $A_{UT}^{sin(2\phi-\phi_S)}$, which arises from the interference term $\bar{E}_T \cdot E$ is found to be zero with the same accuracy. The confirmation of a non-zero asymmetry $A_{UT}^{sin(\phi_S)}$ could provide the first experimental evidence for the chiral-odd (or transversity) GPD H_T.

The x_{Bj}, Q^2 and P_T^2 dependencies of the three target spin asymmetries $A_{UT}^{sin(\phi-\phi_S)}$, $A_{UT}^{sin(2\phi-\phi_S)}$ and $A_{UT}^{sin(\phi_S)}$ are shown in Fig. 18 and compared to the theoretical prediction from [14]. The agreement with the prediction is excellent as function of all three kinematic variables. These results are part of the work of the former PhD student, G. Jegou and post-doc H. Wollny.

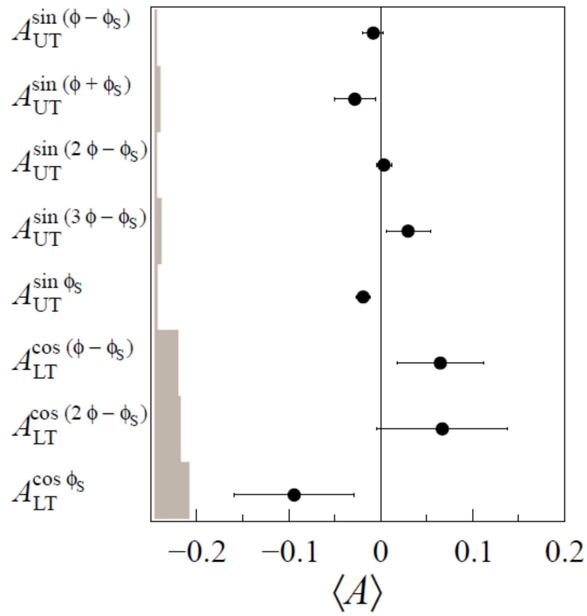

Figure 17: Mean value $< A >$ and the statistical error for every modulation. The error bars (left bands) represent the statistical (systematic) uncertainties.

3 Outlook

The present GPD program focuses on measurements of the GPD H functions only. The GPD E functions, which are of great interest for the Ji sum rule [15], are more difficult to measure. They can be accessed using exclusive reactions on a transversely polarized target. However, with the present COMPASS polarized target such measurements are not feasible. They require a new, or a greatly modified, design of the transversely polarized target.

The new magnet must produce a strong polarizing field, surrounding a large-size target (typically 1.2 m long). In addition, it should also integrate a transverse holding field. More importantly, in order to preserve the recoiling proton detection capabilities, the material budget around the target should be kept extremely low. Such a project presents ambitious technological challenges. The first studies on the design of such superconducting magnet have already been initiated. Further R&D activities should continue within the CryPTA project in the framework of the Hadron Physics Horizon 2020 call.

Besides the studies of a new superconducting magnet, an optimized recoil proton detector, if possible based on the present CAMERA detector, will also be considered. The new detector should provide a good enough momentum resolution and a good capability for low momentum detection. The detailed physics program related to the studies of GPD E is still to be developed. Simulation work on the DVCS and HEMP observables based on the last developed GPD models should start in the very near future.

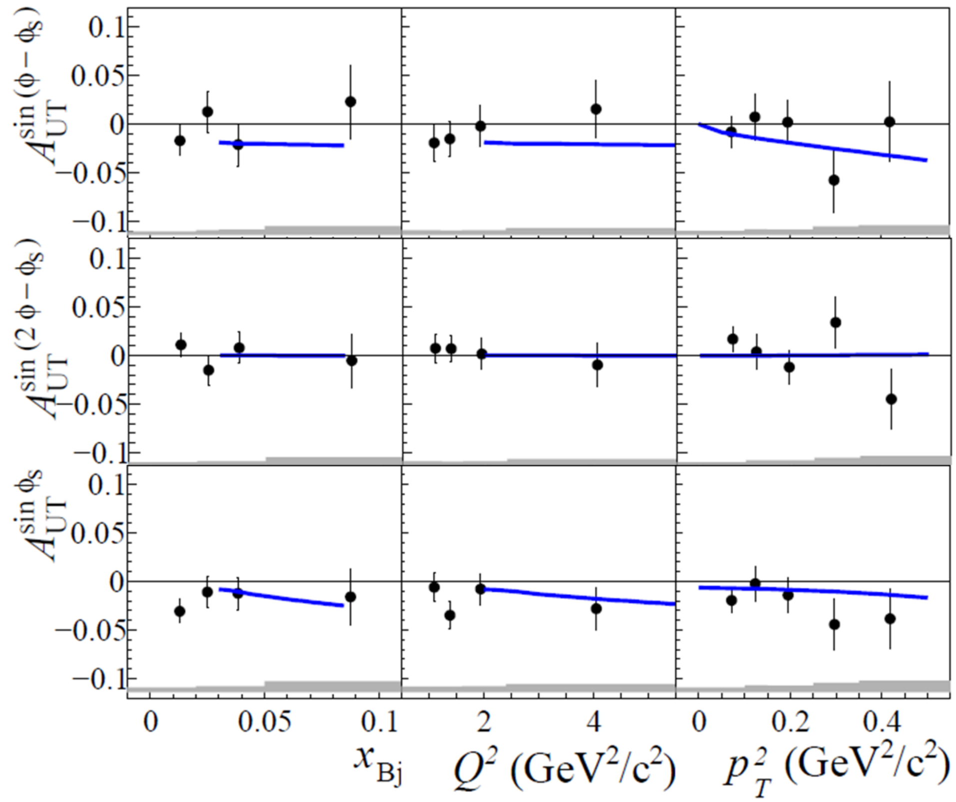

Figure 18: Single-spin azimuthal asymmetries for a transversely (T) polarized target and unpolarized (U) beam. The error bars (grey bands) represent the statistical (systematic) uncertainties. The curves show the predictions of the GPD model [14]

References

[1] COMPASS Collaboration, F. Gautheron et al., CERN-SPSC-2010-014, SPSC-P-340, May 2010.

[2] S. Meissner, A. Metz, M. Schlegel, JHEP **0908**, 056 (2009).

[3] H1 Collaboration, A. Aktas et al., Eur. Phys. J. C **44** (2005) 1;
F.D. Aaron et al., Phys. Lett. B **659** (2008) 796.

[4] ZEUS Collaboration, S. Chekanov et al., JHEP **0905** (2009) 108.

[5] HERMES Collaboration, A. Airapetian et al., JHEP **1210** (2012) 042;
A. Airapetian et al., JHEP **1207** (2012) 032;
A. Airapetian et al., JHEP **06** (2008) 066;
A. Airapetian et al., JHEP **07** (2012) 032.

[6] JLab, C. Munoz Camacho et al., Phys. Rev. Lett. **97** (2006) 262002;
M. Mazouz et al., Phys. Rev. Lett. **99** (2007) 242501;
F.X. Girod et al., Phys. Rev. Lett. **100** (2008) 162002.

[7] Proposals on DVCS at JLab 12 GeV: PR12-06-114, PR12-06-119, E12-11-003.

[8] A. V. Belitsky, D. Mueller, A. Kirchner, Nucl Phys. B **629** (2002) 323.

[9] M. Vanderhaeghen et al., Phys. Rev. D **60** (1999) 094017;
K. Goeke et al., Prog. Part. Nucl. Phys. **47** (2001) 401.

[10] A. V. Belitsky, D. Mueller, Nucl Phys. B **841** (2010) 1.

[11] A. Sandacz and P. Sznajder, HEPGEN, generator for hard exclusive leptoproduction, http://arxiv.org/abs/arXiv:1207.0333.

[12] COMPASS Collaboration, C. Adolph et al., Nucl. Phys. B **865** (2012) 1.

[13] COMPASS Collaboration, C. Adolph et al., Phys. Lett. B **731** (2014) 19.

[14] S.V. Goloskokov and P. Kroll, Eur. Phys. J. C **74** (2014) 2725.

[15] X.-D. Ji, Phys. Rev. Lett. **78**, (1997) 610; Phys. Rev. D **55**, 7114 (1997).